PCCP

PAPER

View Article Online
View Journal | View Issue

Cite this: *Phys. Chem. Chem. Phys.*, 2015, **17**, 22227

Quantifying the origin of inter-adsorbate interactions on reactive surfaces for catalyst screening and design†

Aravind Krishnamoorthy[ab] and Bilge Yildiz*[abc]

The adsorption energy of reactant molecules and reaction intermediates is one of the key descriptors of catalytic activity of surfaces and is commonly used as a metric in screening materials for design of heterogeneous catalysts. The efficacy of such screening schemes depends on the accuracy of calculated adsorption energies under reaction conditions. These adsorption energies can depend strongly on interactions between adsorbed molecules in the adlayer. However, these interactions are typically not accounted for in screening procedures that use DFT-based zero-coverage adsorption energies. Identifying the physical mechanisms behind these interactions is essential to model realistic catalyst surfaces under reaction conditions and to understand the dependence of adsorption energies on reaction parameters like surface strain and composition. This article describes a method to quantitatively resolve the observed inter-adsorbate interactions into various direct adsorbate–adsorbate interactions (*i.e.* Coulombic and steric) and surface-mediated interactions (*i.e.* adsorbate-induced surface relaxation and change in electronic structure) by combining density functional theory and cluster-expansion calculations of coverage-dependent adsorption energies. The approach is implemented on a model catalyst surface of FeS_2(100) reacting with H_2S molecules. We find that the adsorption energy of H_2S molecules can be affected by over 0.55 eV by the repulsive inter-adsorbate interactions caused primarily by the adsorbate-induced changes to the electronic structure of the FeS_2 surface. These interactions also show a strong monotonic dependence on surface strain, being three times stronger on compressively strained surfaces than on surfaces under tensile strain. The large magnitude of inter-adsorbate interactions as well as their strong dependence on lattice strain demonstrate the need for using coverage-dependent adsorption energies for more accurate screening, for example for strained catalytic systems like core–shell and overlayer structures.

Received 31st May 2015,
Accepted 27th July 2015

DOI: 10.1039/c5cp03143e

www.rsc.org/pccp

Introduction

High throughput screening of materials for heterogeneous catalysis is rapidly becoming an important part of the catalyst selection and design process. In this paradigm, the Sabatier principle and Brønsted–Evans–Polanyi scaling relations are used to infer surface activity from the adsorption energy of reactant molecules and reaction intermediates.[1,2] This approach is especially attractive for identifying promising material combinations for systems like core–shell and overlayer catalysts, where variables like surface strain and choice of alloying elements can be used to systematically tune the adsorption energy and, therefore, the activity of the surface. The efficacy of such screening procedures depends on the ability to accurately model the catalyst surface under reaction conditions and calculate the appropriate adsorption energies. Usually, these adsorption energies are calculated *ab initio* in simulation cells that contain a single reactant molecule on a surface that is laterally large enough to eliminate adsorbate–adsorbate interactions. This simplistic 'zero-coverage' picture of the reacting surface differs greatly from real catalyst surfaces that contain a finite surface coverage of reactant molecules in that it does not include interactions between adsorbed species in the adlayer.

Strong inter-adsorbate interactions have been observed on a variety of reaction systems, such as H_2O/TiO_2(110),[3] CO/Ru(0001),[4] and O on the (111) surface of several transition metals.[5] These interactions result in effective adsorption energies that are significantly different from values at zero-coverage and are, in some cases, strong enough to cause surface restructuring and roughening.[6] These modified adsorption energies can

[a] *Laboratory for Electrochemical Interfaces, Massachusetts Institute of Technology, Cambridge, MA 02139, USA*
[b] *Department of Materials Science and Engineering, Massachusetts Institute of Technology, Cambridge, MA 02139, USA*
[c] *Department of Nuclear Science and Engineering, Massachusetts Institute of Technology, Cambridge, MA 02139, USA. E-mail: byildiz@mit.edu*

† Electronic supplementary information (ESI) available. See DOI: 10.1039/c5cp03143e

not only alter the activity of surfaces along the Sabatier 'volcano' curve,[7] but can also alter the shape of the curve itself leading to a pronounced flattening near the peak activity.[8] Previous studies into the effect of inter-adsorbate interactions have been mostly limited to quantification of the total magnitude of these interactions.[9,10] While such studies lead to a better representation of the catalytic activity, the physical basis of these interactions is under-investigated, without a quantitative understanding of their dependence on variables like surface strain and composition.

Ab initio calculations can help isolate the mechanism behind inter-adsorbate interactions, but a very large configurational sample space of adsorbed surface sites must be sampled to identify ground-state configurations. Since a brute-force sampling of the entire configurational space is computationally intractable for all but the smallest supercells, past studies for quantifying the magnitude of these interactions have typically resorted to a random sampling of the configurational space[9] or using a more rigorous statistical sampling method like cluster expansion.[10] In both cases, efforts have focused on quantifying the total magnitude of inter-adsorbate interactions rather than on uncovering the dominant mechanism behind these interactions, which is more useful in providing design rules for catalyst surfaces.

In this article, we report investigations into the nature and strength of inter-adsorbate interactions, demonstrated on a model system of H_2S adsorbates on the pyrite $FeS_2(100)$ surface. We use density functional theory (DFT) and cluster expansion methods to calculate adsorption energies as a function of surface coverage. We chose this model system because the interaction of adsorbate species with the (100) surface of FeS_2 is of interest in several fields including heterogeneous catalysis[11,12] and photovoltaics,[13] and the importance of H_2S as a reactant species is well established in areas of corrosion[14] and biogeochemistry.[15] The rest of the paper is structured as follows. In the first two sections, the methodology used to calculate adsorption and interaction energies is briefly described followed by the computational details. The next section is devoted to quantifying the contribution of different types of forces, *i.e.* Coulombic and Pauli repulsion, and different mechanisms, *i.e.* adsorbate-induced surface relaxation and adsorption-induced change of surface electronic structure, to the overall inter-adsorbate interaction. In the final section, the framework is applied to the study of adsorption on biaxially strained $FeS_2(100)$ surfaces to extract adsorption energies under conditions of finite coverage and finite surface strain. We conclude by listing briefly some implications of the current work for the selection and design of strained and unstrained catalyst surfaces.

Methodology

We briefly describe below the framework adopted[16,17] to quantify inter-adsorbate interactions from a calculation of adsorption energies at different coverage values, and introduce some terms that are used frequently in the rest of the article. This is followed by a discussion about the need for cluster expansion sampling in obtaining these adsorption energies. We then apply this framework to carefully chosen adsorbate/surface systems, closely related to the $H_2S/FeS_2(100)$ system, in order to isolate the influence of individual mechanisms on the overall interaction. The considered mechanisms include both direct adsorbate–adsorbate and surface-mediated interactions.

On a catalyst surface containing M adsorption sites, the cumulative adsorption energy of n adsorbates (defined as the sum of adsorption energies of n adsorbates) of species X, corresponding to a surface coverage of $\theta = \frac{n}{M}$ monolayer, is given by

$$E_{\mathrm{ads}}^{\mathrm{sum}}\left(\theta = \frac{n}{M}\right) = E_{\mathrm{S}-n\mathrm{X}} - E_{\mathrm{S}} - (n \cdot E_{\mathrm{X}}) \qquad (1)$$

where $E_{\mathrm{S}-n\mathrm{X}}$ is the DFT-calculated energy of the system containing n molecules of species X that are adsorbed to the catalyst surface, E_{S} is the energy of the bare catalyst surface, and E_{X} is the energy of an isolated molecule of species X. In the absence of any interactions between adsorbates (direct or surface-mediated), the cumulative adsorption energy will be a linear function of the surface coverage. Therefore, one simple way to measure the magnitude of inter-adsorbate interactions is to subtract zero-coverage contributions from $E_{\mathrm{ads}}^{\mathrm{sum}}(\theta)$ to obtain the cumulative inter-adsorbate interaction, $E_{\mathrm{inter}}^{\mathrm{sum}}(\theta)$ (eqn (2)).

$$E_{\mathrm{inter}}^{\mathrm{sum}}(\theta) = E_{\mathrm{ads}}^{\mathrm{sum}}(\theta) - (\theta \cdot E_{\mathrm{ads}}(0)) \qquad (2)$$

For direct comparison with experiments, a more useful quantity is the binding energy or the effective adsorption energy at a given coverage, $E_{\mathrm{ads}}\left(\theta = \frac{n}{M}\right)$, which can be derived from eqn (1) using

$$E_{\mathrm{ads}}\left(\theta = \frac{n}{M}\right) = \frac{\mathrm{d}\left[E_{\mathrm{ads}}^{\mathrm{sum}}(\theta)\right]}{\mathrm{d}\theta} \qquad (3)$$

Calculating the adsorption energy using eqn (1) and (3) is not straightforward because $E_{\mathrm{S}-n\mathrm{X}}$ is not unique for a given value of n ($n \neq 0, M$), since there are several configurational arrangements of adsorbates on the available adsorption sites each resulting in a different value of $E_{\mathrm{S}-n\mathrm{X}}$. Since adsorbates are highly mobile at operating temperatures, of most interest to this study is the configuration which results in the lowest $E_{\mathrm{S}-n\mathrm{X}}$ for a given surface coverage. Identification of these *a priori* unknown ground states is a challenging problem since a brute-force sampling of the entire adsorbate configurational space is computationally intractable for all but the smallest simulation cells, and a random sampling of the configurations[9] is not guaranteed to identify all ground states. Instead, we implement the cluster expansion method,[10,18] as applied previously to other adsorbate systems like NO/Pt(111)[19] and H/graphene,[20] to construct a Ising-like Hamiltonian of the adlayer using DFT-calculated energies of a subset of adsorbate configurations. This Hamiltonian is then used to predict ground state configurations at different coverages, whose energies are explicitly calculated using DFT.

To measure the contribution of individual forces and mechanisms to the overall inter-adsorbate interaction in the H_2S/FeS_2 system, $E_{\mathrm{ads}}(\theta)$ and $E_{\mathrm{inter}}^{\mathrm{sum}}(\theta)$ are compared among closely related adsorbate/surface systems. These related systems are created by

altering one aspect of the original H_2S/FeS_2 system at a time, such as the rigidity or strain state of the surface or replacing the H_2S adsorbates by H atoms. The different mechanisms investigated in this work and the corresponding adsorbate/surface systems are discussed in more detail in the Results and discussion section.

Computational details

All DFT calculations[21] in this study were performed with the Vienna Ab initio Simulation Package[22,23] using the spin-polarized PBE functional[24] and atomic potentials generated by the projector augmented wave method.[25] To correct for electronic self-correlation effects commonly found in 3d transition metal compounds, we adopt the DFT+U method,[26] with a U–J value of 1.6 eV for the Fe 3d electrons, determined to be appropriate for iron sulfide phases.[27] Cluster expansion calculations were carried out using the MIT *ab initio* Phase Stability[28] code included as part of the Alloy Theoretic Automated Toolkit.[29] Adsorbate configurations were sampled with 1, 2 and 3 points per cluster and the one-removed cross-validation score is less than 0.03 eV in the case of H_2S adsorbates and 0.01 eV in the case of H adsorbates, indicating good predictive power of the cluster expansion to generate thermodynamically accurate ground state adsorbate configurations.

All adsorption energies are calculated on 4 layer pyrite FeS_2 slabs of 2×2 unit-cell lateral size, separated by 10 Å of vacuum in a periodic simulation cell. Each simulation cell contains 32 formula units of pyrite. Wave functions are expanded in plane waves with kinetic energies up to 350 eV and the reciprocal space was sampled using $3 \times 3 \times 1$ Monkhorst–Pack grids.[30] This choice of plane-wave energies and Brillouin-zone sampling grids leads to well-converged adsorption energies over the entire range of surface coverage, $\theta \in [0,1]$ (Fig. S4 and S5, ESI†). Total energies are converged to within 5×10^{-5} eV in each self-consistency cycle and the forces on ions were converged to within 0.05 eV Å^{-1}.

We confirm the accuracy of the calculated adsorption energies by using a program[31] to perform a simulation of temperature programmed desorption of H_2S from the $FeS_2(100)$ surface. The program generates the TPD spectrum by numerically solving the differential equation describing the dependence of surface coverage on temperature in the first-order desorption process:

$$\frac{d\theta}{dT} = -\frac{A}{\beta}\exp\left(\frac{E_{ads}(\theta)}{k_B T}\right)\theta$$

where A is the Arrhenius pre-exponential factor (assumed to be 10^{13} s^{-1}, in the limit of an immobile transition state during desorption[32]), β is the experimental heating rate,[33] k_B is the Boltzmann constant and T is the absolute temperature.

All images of crystal structures used in this article were generated using the VESTA structural visualization program.[34]

Results and discussion

The non-dissociative adsorption of the weakly nucleophilic H_2S molecules occurs on the eight Fe ions exposed at the 2×2 $FeS_2(100)$ surface, where the LUMO of the pyrite surface is localized.[35,36] The resulting Fe–SH_2 bond has a bond length of 2.30 Å (at all coverage values), which is similar to the Fe–S bond lengths in the bulk of the FeS_2 crystal (2.25 Å). H_2S adsorption saturates the dangling bond on the Fe ion by completing the Fe–S_6 octahedron, leading to a change of the electronic structure of the FeS_2 surface.

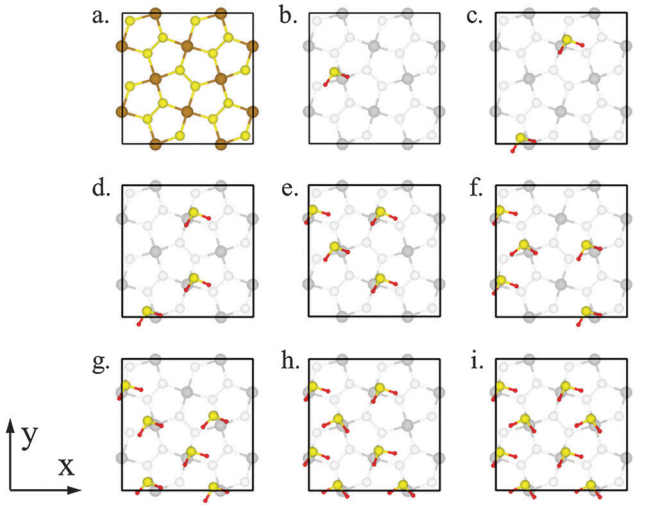

Fig. 1 (a) Atomic structure of the $FeS_2(100)$ surface showing 8 non-equivalent adsorption sites, Fe^{2+} ions (brown) and 16 S^{-} ions (yellow). (b–i) Adsorption configurations at increasing surface coverage values in steps of 12.5% predicted by cluster expansion.

While the adsorbed H_2S molecule is free to rotate about the rigid Fe–SH_2 bond, the inter-adsorbate separation is determined by the distance between the adsorption sites and is independent of surface coverage (Fig. 1). On the $FeS_2(100)$ surface, this results in a nearest-neighbor S–S distance of just 3.4 Å, which is close to twice the van der Waals radius of sulfur (1.8 Å[37]), indicating the presence of direct non-bonding interactions between adsorbates.

In the following sections, we quantify the overall strength of inter-adsorbate interactions between H_2S molecules (Section I) and identify both direct adsorbate–adsorbate as well as surface-mediated mechanisms that contribute to the overall interaction (Section II).

I. Coverage-dependent adsorption energy on $FeS_2(100)$

The cumulative adsorption energy, $E_{ads}^{sum}(\theta)$ for the H_2S adsorbate ground-state structures (Fig. 1) predicted by cluster expansion can be well-fitted by the quadratic expression in Fig. 2a, where a negative energy indicates exothermic adsorption and the deviation towards positive energies indicates the presence of repulsive interactions that lead to weaker binding at higher surface coverages.

The dashed straight-line in Fig. 2a describes the expected behavior of a system with no inter-adsorbate interactions, as represented by the second term in RHS of eqn (2). Subtracting this from the DFT-calculated energy, we get a measure of the total inter-adsorbate interaction energy, $E_{inter}^{sum}(\theta)$ in Fig. 2b. For comparison with experiments, the corresponding binding

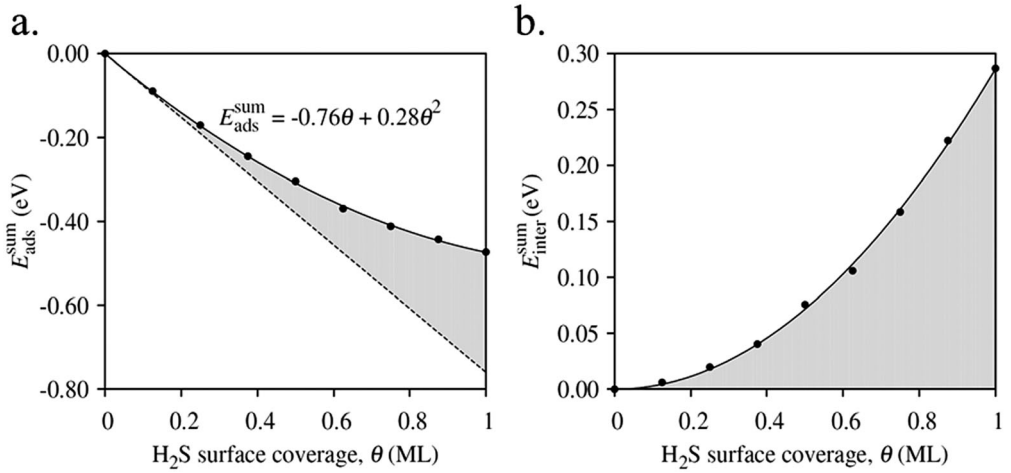

Fig. 2 (a) The sum of adsorption energy deviates from ideal linear behavior at higher coverage values, indicating the presence of repulsive inter-adsorbate interactions (shaded region). (b) Removing the linear component from (a) reveals the quadratic form of the inter-adsorbate interaction energy, E_{inter}^{sum}.

energy or the effective adsorption energy per molecule, $E_{ads}(\theta)$ is calculated by taking the derivative of $E_{ads}^{sum}(\theta)$.

$$E_{ads}(\theta) = \frac{\partial\left[E_{ads}^{sum}(\theta)\right]}{\partial\theta} = -0.76 + 0.56\theta \text{ eV} \qquad (4)$$

To validate the adsorption energy calculated in eqn (4) we simulated the outcome of a temperature programmed desorption (TPD) experiment for H_2S adsorption on the defect-free pyrite (100) surface. We choose simulation parameters like the initial dosing temperature (79 K) and the heating rate (8 K s^{-1}) to be the same as the experimental conditions used by Guevremont *et al.* for the TPD of H_2S from the (100) surface of pyrite.[33] In comparing the simulated TPD results with experimental data of Guevremont *et al.*, we find that the adsorption energies derived from the cluster-expansion approach generates a desorption spectrum that is well-matched with the experimental one in terms of reproducing the broad width of the peak. In contrast, if a single value of adsorption energy (obtained for zero-coverage) is used throughout the TPD, a very different, narrow peak shape is predicted (Fig. 3).

Simulated TPD using adsorption energies from the cluster-expansion method is also in better agreement with the experiment than the TPD calculated using adsorption energies derived from a random sampling of the adsorbate configurational space (Fig. S3, ESI†). This result demonstrates the importance of identifying finite-coverage ground state configurations rigorously using cluster expansion, and the reliability of the cluster-expansion procedure for calculating coverage-dependent adsorption energies.

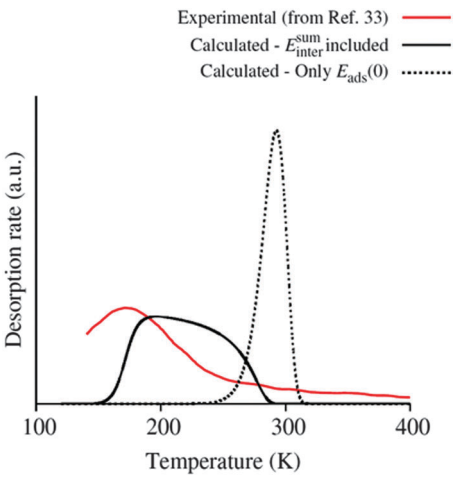

Fig. 3 The calculated TPD spectrum based on coverage dependent adsorption energies deduced by the cluster expansion method has a much closer fit to the experimental spectrum compared to the calculated TPD spectrum based on adsorption energies that do not consider inter-adsorbate interactions. The comparison is made both in terms of the onset temperature for desorption and the temperature range for the desorption process. The curves are normalized by the area under the curve.

II. Mechanisms responsible for inter-adsorbate interactions

It can be seen that the cumulative adsorption energy in Fig. 2 increases, *i.e.* becomes less negative and exothermic, with increasing surface coverage, indicating a repulsive effective interaction between H_2S adsorbates. More significantly, the cumulative adsorption energy depends quadratically on the surface coverage. This quadratic dependence has previously been observed in lattice gas model Hamiltonians that include pair-wise interactions between adsorbed species.[38] Depending upon the adsorbate/surface pair, several physical mechanisms have been shown in literature to be responsible for pairwise inter-adsorbate interactions. We consider four mechanisms here.

1. Coulombic repulsion between charged adsorbates, as seen in O/Pd(111),[39]

2. Through-space steric interactions between adsorbates, as observed in the NO/Pd(111) system,[40]

3. Adsorbate-induced surface-stresses resulting in surface-mediated elastic interaction between adsorbates, as seen in Cl/Au(111),[41] and

4. Adsorbate-induced altering of the electronic structure of neighboring adsorption sites, such as in S/Rh(001).[42]

It is likely that a combination of the above mechanisms is responsible for the observed inter-adsorbate interactions on the $FeS_2(100)$ surface. In the following sections, the magnitude of each contribution is quantified by calculating $E_{ads}^{sum}(\theta)$ and $E_{inter}^{sum}(\theta)$ for different adsorbate-surface systems that allow us to isolate the effect of each mechanism.

a. Coulombic repulsion. Chemisorption of H_2S on $FeS_2(100)$ is accompanied by charge transfer between the adsorbed molecule and the surface, which may result in Coulombic interactions between the adsorbates. To quantify this interaction, the partial charge present on adsorbates was identified by performing a Bader charge analysis[43] on adsorbed and isolated H_2S molecules. We found that the adsorbed H_2S molecules are nearly electrically neutral with residual charge of $0.06 \pm 0.02\ e^-$ compared to isolated molecules (Fig. S1, ESI†). To identify if Coulombic interactions are a source of significant inter-adsorbate interactions in the $H_2S/FeS_2(100)$ system, we compare it to interactions in the atomic $H/FeS_2(100)$ system. This is useful because atomic H adsorbates have a Bader charge of $-0.13 \pm 0.01\ e^-$, and are therefore expected to exhibit Coulombic interactions of similar magnitude to H_2S molecules. Unlike the H_2S adsorbates, atomic H adsorbates show no observable inter-adsorbate interaction (Fig. 4). Therefore, the contribution of Coulombic repulsion to the overall interactions among H_2S adsorbates is expected to be negligible.

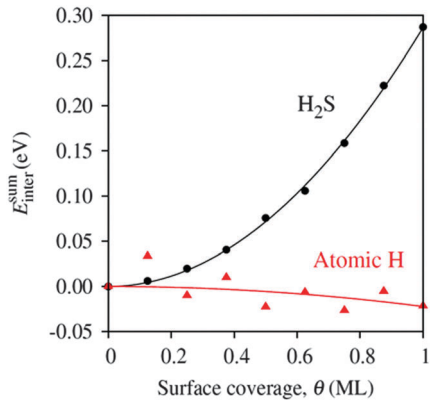

Fig. 4 H_2S and atomic H adsorbates that have the same charge around $0.1\ e^-$, show very different interaction strengths within their corresponding adlayers. This indicates that Coulombic interactions (which scale with adsorbate charge) are only minor contributors to the inter-adsorbate interaction in the H_2S adlayer.

b. Through-space steric interactions. Spatially large molecules also sterically block the adsorption of other molecules on neighboring adsorption sites by penalizing the non-bonding overlap of the electron clouds of nearby adsorbates. This mechanism is also operative in the H_2S/FeS_2 system, where it is observed that the electronic charge in the adlayer is redistributed away from an incoming H_2S adsorbate (Fig. 5a).

To quantify the effect of Pauli repulsion, $E_{inter}^{sum}(\theta)$ was calculated for systems in the absence of the $FeS_2(100)$ surface. Since this eliminates the possibility of any surface-mediated effects, the only interactions captured in these calculations are through-space steric effects (Coulombic effects do not come into play because the molecules are identically uncharged). It was found that steric effects account for a measurable, but still a minor part ($\approx$10%) of the overall inter-adsorbate interactions between adsorbed H_2S molecules (Fig. 5b).

c. Adsorbate-induced surface stresses. Adsorbates can also induce local surface stresses that lead to relaxation of neighboring adsorption sites, potentially affecting the adsorption energy of subsequent adsorbates. To understand this effect, inter-adsorbate interaction energies, $E_{inter}^{sum}(\theta)$, are compared for two related systems; one where the Fe and S atoms in the surface are allowed to relax in response to H_2S adsorption and another one where they are held in fixed positions. The latter system does not contain any adsorbate-induced surface stress within the FeS_2. Therefore, a difference in the $E_{inter}^{sum}(\theta)$ between these two systems gives us a measure of the contribution of elastic interactions on the catalyst surface towards the overall

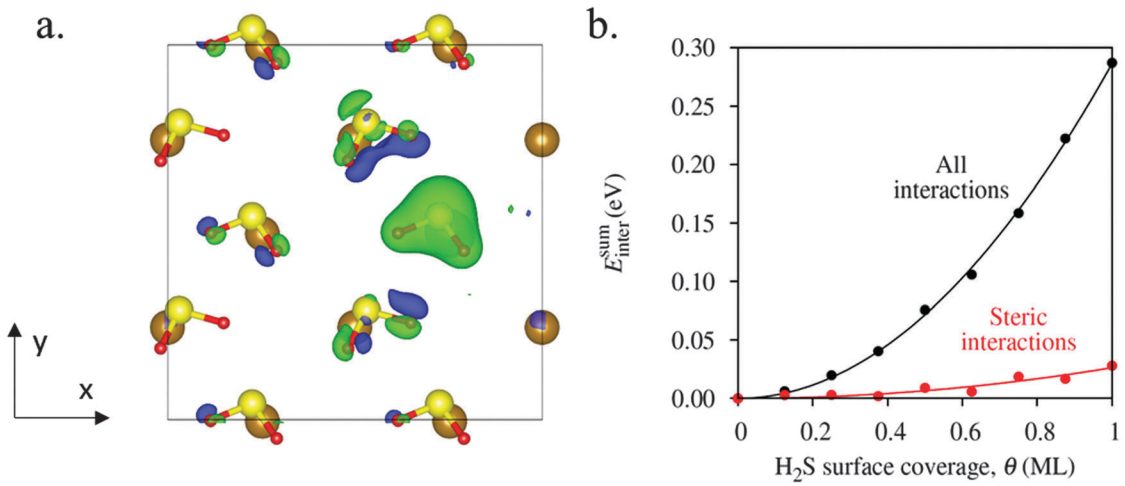

Fig. 5 (a) Electron density isosurfaces indicate that Pauli repulsion is responsible for redistributing electrons (green) away from the newly adsorbed H_2S molecule creating a region of depleted electron density (blue). (b) Pauli repulsion contributes to only about 10% of the overall inter-adsorbate interaction seen in the $H_2S/FeS_2(100)$ system.

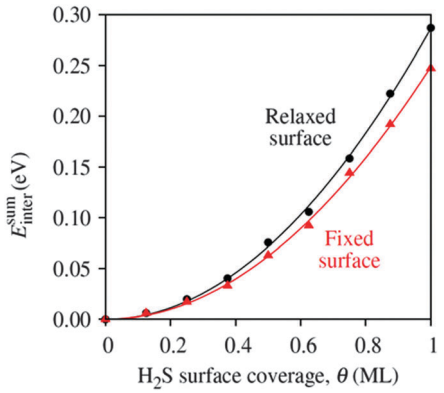

Fig. 6 The magnitude of inter-adsorbate interaction remains largely unchanged regardless of the relaxation of the surface, indicating that the surface-mediated elastic effects contribute only marginally to the overall inter-adsorbate interaction for the $H_2S/FeS_2(100)$ system.

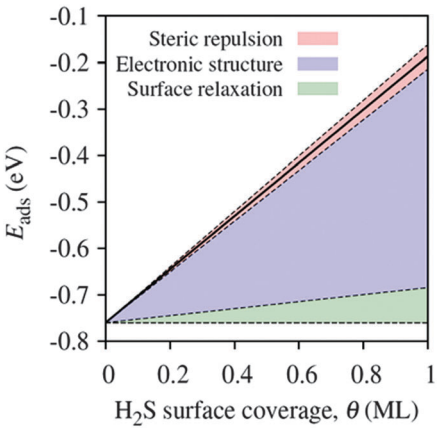

Fig. 7 Adosrbate-induced changes to surface electronic structure are largely responsible for the coverage dependence of adsorption energy in the $H_2S/FeS_2(100)$ system. Both the surface elastic relaxation and Pauli repulsion are minor contributions to the overall inter-adsorbate interaction.

inter-adsorbate interaction. Although H_2S adsorption causes noticeable relaxation of the $FeS_2(100)$ surface, the observed interaction energies are very similar for both the rigid and relaxed surfaces, indicating that the contribution of surface-mediated elastic interactions within FeS_2 is not significant in this system (Fig. 6).

d. Adsorbate-induced change of surface electronic structure. In addition to charge transfer, formation of the adsorbate-surface bond alters the electronic structure of the surface, which, in turn, affects the adsorption energy of the subsequent adsorbates. To quantitatively capture this influence on the effective inter-adsorbate interaction, two pieces of information are required.

i. A metric that measures the change in electronic structure due to increasing H_2S coverage, and

ii. A dependence of the H_2S adsorption energy on this surface electronic structure metric.

We perform a two-part calculation to obtain these pieces of information. Since H_2S molecules adsorb on the Fe^{2+} sites on the pyrite surface, we use the distance between the Fe 3d band and the Fermi level calculated from the Density of States as a metric to represent the electronic structure of the surface, as prescribed by the widely adopted d-band theory.[44] In the first step, we calculate the Density of States at different H_2S coverages and observe the dependence of this metric on surface coverage. In the second step, to understand how the surface electronic structure affects H_2S adsorption, the surface electronic structure metric is systematically and controllably varied by imposing lateral strain on the $FeS_2(100)$ surface and the corresponding zero-coverage adsorption energy is calculated. A product of these two dependencies (Fig. S2, ESI†) quantifies the contribution of adsorbate-induced electric structure change on the overall inter-adsorbate interaction (eqn (5)).

$$\frac{dE_{ads}}{d\theta} = \frac{dE_{ads}}{dE_{DBC}} \cdot \frac{dE_{DBC}}{d\theta} \quad (5)$$

where E_{DBC} is the electronic structure metric derived from the d-band theory and E_{ads} and θ have their usual meanings as previously described.

A summary of contributions from all the individual forces and mechanisms considered in this study (Fig. 7) clearly demonstrates that the altered surface electronic structure is the largest factor to the observed dependence of adsorption energy on surface coverage. Since the independently computed contributions very nearly sum up to the overall observed interaction (denoted by the thick line in Fig. 7), any forces not considered in this study (*i.e.* van der Waals) are expected to be relatively minor contributions.

III. Inter-adsorbate interaction on biaxially strained surfaces

The dependence of the 'zero-coverage' adsorption energy on the strain state of the catalyst surface is well-established, and elastic strain is understood to be an important variable in several catalytic systems.[45–47] However, the impact of lattice strain on the interactions within the adlayer has not been explored so far, to our knowledge. Quantifying the role of strain on inter-adsorption interactions and understanding its impact on the different interaction mechanism that were presented above can allow us to exploit lattice strain accurately as an important parameter in catalyst selection.

To elucidate the role of strain, the cumulative inter-adsorbate energy, $E_{inter}^{sum}(\theta)$ is calculated as described in the Methodology section for H_2S adsorbates on $FeS_2(100)$ surfaces under biaxial strains, ε ($=\varepsilon_{xx} = \varepsilon_{yy}$) ranging from -0.05 to 0.05 in steps of 0.025. Fig. 8a shows that inter-adsorbate interactions strengthen monotonically with closer packing of adsorption sites as the lattice strain is varied from 0.05 (tensile) to -0.05 (compressive). Quantitatively, interactions on the most compressively strained surface are three times stronger than on the most tensile strained surface. This increasing interaction translates to a greater dependence of adsorption energy on surface coverage with increasing compressive strain. The most immediate implication of this interplay is that the variation of adsorbate binding energy with elastic surface strain is significantly different at finite coverage values than at zero coverage. For instance, the difference in adsorption energies of a H_2S molecule on the unstrained and 5% tensile strained FeS_2 surface is less than 0.05 eV at zero coverage but expands to over 0.30 eV at 1 monolayer coverage (Fig. 8b).

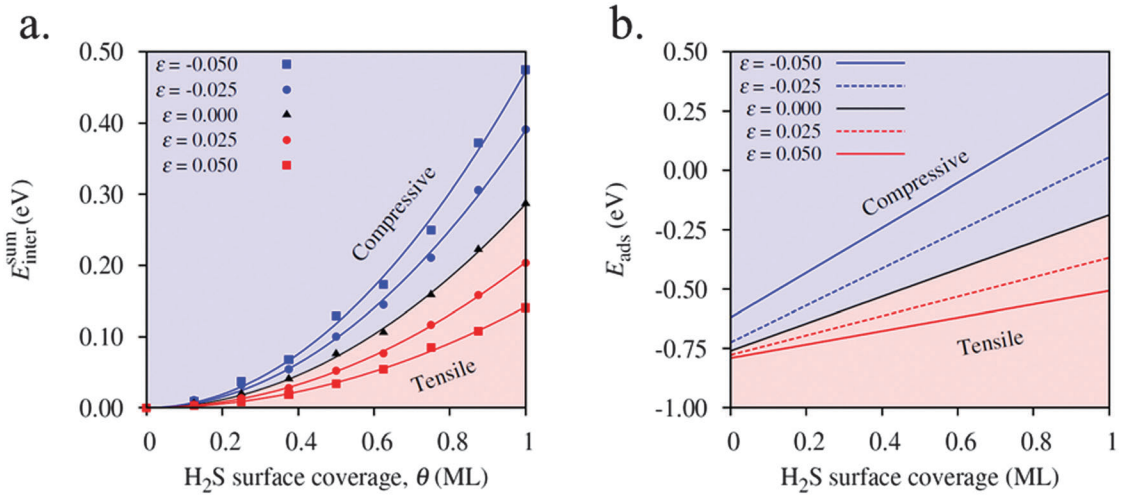

Fig. 8 (a) Inter-adsorbate interactions among H_2S adsorbates are stronger on the compressively strained $FeS_2(100)$ surface compared to the unstrained surface or the tensile strained surface. (b) Increased inter-adsorbate interactions on the compressively strained surface are reflected as a stronger dependence (larger slope) of adsorption energy on surface coverage.

Summary and conclusion

We quantified the magnitude of inter-adsorbate interactions by using DFT and cluster expansion method, and by selected modifications of the surface to allow for isolating the magnitude of each interaction mechanism. The coverage-dependent adsorption energies and the contributing mechanisms were demonstrated for H_2S molecules on the $FeS_2(100)$ surface. We further resolved these interactions into contributions from direct steric and Coulombic repulsion among the adsorbates, as well as indirect interactions due to adsorbate-induced change of electronic structure and surface relaxation.

On the FeS_2 surface, repulsive interactions between H_2S molecules, arising mainly from changes in the surface electronic structure were found to affect the H_2S adsorption energy by over 0.55 eV. Inter-adsorbate interactions also show a strong dependence on the biaxial strain on the surface, with compressively strained surfaces exhibiting the strongest inter-adsorbate interactions. The large magnitude of these inter-adsorbate interactions as well as their strong dependence on experimental parameters like surface strain highlight the need for moving beyond 'zero-coverage' adsorption energies in the material screening process, especially for strained catalyst systems. Towards this end, the identification and quantification of individual contributions to the inter-adsorbate interactions described in this work can help understand how adsorption energies on realistic surfaces vary with experimental conditions, enables more accurate surface reaction kinetic models, and provides for better-informed screening of materials for heterogeneous catalysis applications.

Acknowledgements

We gratefully acknowledge support provided by BP PLC through the BP-MIT Center for Materials and Corrosion Research and by the National Science Foundation for the computational resources provided through the Texas Advanced Computing Center under Grant No. TG-DMR120025. We thank William Herbert, Mostafa Youssef and Dario Marrocchelli for useful discussions.

References

1 J. K. Nørskov, T. Bligaard, J. Rossmeisl and C. H. Christensen, *Nat. Chem.*, 2009, **1**, 37–46.
2 J. Greeley, T. F. Jaramillo, J. Bonde, I. B. Chorkendorff and J. K. Norskov, *Nat. Mater.*, 2006, **5**, 909–913.
3 P. Lindan and C. Zhang, *Phys. Rev. B: Condens. Matter Mater. Phys.*, 2005, **72**, 075439.
4 T. Diemant, H. Rauscher, J. Bansmann and R. J. Behm, *Phys. Chem. Chem. Phys.*, 2010, **12**, 9801–9810.
5 S. D. Miller, N. Inoğlu and J. R. Kitchin, *J. Chem. Phys.*, 2011, **134**, 104709.
6 C. Aldao, S. Guidoni, G. Xu, K. Nakayama and J. Weaver, *Surf. Sci.*, 2004, **551**, 143–149.
7 L. C. Grabow, B. Hvolbaek and J. K. Norskov, *Top. Catal.*, 2010, **53**, 298–310.
8 L. Qi and J. Li, *J. Catal.*, 2012, **295**, 59–69.
9 J. Kitchin, *Phys. Rev. B: Condens. Matter Mater. Phys.*, 2009, **79**, 205412.
10 D. Lerch, O. Wieckhorst, L. Hammer, K. Heinz and S. Muller, *Phys. Rev. B: Condens. Matter Mater. Phys.*, 2008, **78**, 121405.
11 R. Murphy and D. R. Strongin, *Surf. Sci. Rep.*, 2009, **64**, 1–45.
12 M. Sacchi, M. C. E. Galbraith and S. J. Jenkins, *Phys. Chem. Chem. Phys.*, 2012, **14**, 3627–3633.
13 Y. Bi, Y. Yuan, C. L. Exstrom, S. A. Darveau and J. Huang, *Nano Lett.*, 2011, **11**, 4953–4957.
14 H. Vedage, T. A. Ramanarayanan, J. D. Mumford and S. N. Smith, *Corrosion*, 1993, **49**, 114–121.
15 K. R. Popper, *Nature*, 1990, **344**, 387.
16 X. Guo, W. Liu, W. Fang, L. Cai, Y. Zhu, L. Lu and X. Lu, *Phys. Chem. Chem. Phys.*, 2012, **14**, 16618–16625.

17 T. Wang, X. Tian, Y. Li, J. Wang, M. Beller and H. Jiao, *Acs Catal.*, 2014, **4**, 1991–2005.
18 J. Sanchez, F. Ducastelle and D. Gratias, *Phys. A*, 1984, **128**, 334–350.
19 C. Wu, D. Schmidt, C. Wolverton and W. Schneider, *J. Catal.*, 2012, **286**, 88–94.
20 H. Xiang, E. Kan, S. Wei, X. Gong and M. Whangbo, *Phys. Rev. B: Condens. Matter Mater. Phys.*, 2010, **82**, 165425.
21 W. Kohn and L. J. Sham, *Phys. Rev.*, 1965, **140**, A1133.
22 G. Kresse and J. Furthmüller, *Comput. Mater. Sci.*, 1996, **6**, 15–50.
23 G. Kresse and J. Furthmüller, *Phys. Rev. B: Condens. Matter Mater. Phys.*, 1996, **54**, 11169.
24 J. P. Perdew, K. Burke and M. Ernzerhof, *Phys. Rev. Lett.*, 1996, **77**, 3865.
25 P. E. Blöchl, *Phys. Rev. B: Condens. Matter Mater. Phys.*, 1994, **50**, 17953.
26 S. L. Dudarev, G. A. Botton, S. Y. Savrasov, C. J. Humphreys and A. P. Sutton, *Phys. Rev. B: Condens. Matter Mater. Phys.*, 1998, **57**, 1505.
27 A. Krishnamoorthy, F. W. Herbert, S. Yip, K. J. Van Vliet and B. Yildiz, *J. Phys.: Condens. Matter*, 2013, **25**, 045004.
28 A. van de Walle and G. Ceder, *J. Phase Equilib.*, 2002, **23**, 348–359.
29 A. van de Walle, M. Asta and G. Ceder, *CALPHAD: Comput. Coupling Phase Diagrams Thermochem.*, 2002, **26**, 539–553.
30 H. J. Monkhorst and J. D. Pack, *Phys. Rev. B: Condens. Matter Mater. Phys.*, 1976, **13**, 5188.
31 The source code for the FORTRAN program used to perform TPD simulations is available at https://github.com/arvk/h2s-fes2-tpd. Some scripts for visualization of the TPD spectrum are also provided.
32 J. A. Dumesic, *The Microkinetics of Heterogeneous Catalysis*, American Chemical Society, Washington, D.C., 1993.
33 J. M. Guevremont, D. R. Strongin and M. A. A. Schoonen, *Am. Mineral.*, 1998, **83**, 1246–1255.
34 K. Momma and F. Izumi, *J. Appl. Crystallogr.*, 2008, **41**, 653–658.
35 G. Qiu, Q. Xiao, Y. Hu, W. Qin and D. Wang, *J. Colloid Interface Sci.*, 2004, **270**, 127–132.
36 A. Stirling, M. Bernasconi and M. Parrinello, *J. Chem. Phys.*, 2003, **118**, 8917–8926.
37 M. Mantina, A. Chamberlin, R. Valero, C. Cramer and D. Truhlar, *J. Phys. Chem. A*, 2009, **113**, 5806–5812.
38 T. Juwono, I. Abou Hamad, P. Rikvold and S. Wang, *J. Electroanal. Chem.*, 2011, **662**, 130–136.
39 M. Todorova, K. Reuter and M. Scheffler, *Phys. Rev. B: Condens. Matter Mater. Phys.*, 2005, **71**, 195403.
40 Z. Zeng, J. Da Silva and W. Li, *Phys. Rev. B: Condens. Matter Mater. Phys.*, 2010, **81**, 085408.
41 R. Xie, D. Chen, X. Wang, T. He and F. Liu, *J. Phys. Chem. B*, 2002, **106**, 12948–12956.
42 P. J. Feibelman and D. R. Hamann, *Phys. Rev. Lett.*, 1984, **52**, 61–64.
43 W. Tang, E. Sanville and G. Henkelman, *J. Phys.: Condens. Matter*, 2009, **21**, 084204.
44 B. Hammer and J. K. Nørskov, *Nature*, 1995, **376**, 238–240.
45 M. Mavrikakis, B. Hammer and J. K. Norskov, *Phys. Rev. Lett.*, 1998, **81**, 2819–2822.
46 M. Gsell, P. Jakob and D. Menzel, *Science*, 1998, **280**, 717–720.
47 A. Kushima, S. Yip and B. Yildiz, *Phys. Rev. B: Condens. Matter Mater. Phys.*, 2010, **82**, 115435.

